This paper received the *Best Paper Award* at the 7th Ansys conference in Pittsburgh, PA, USA, May 20-22, 1996

PIEZOELECTRIC SIMULATIONS VALIDATED ON BEAMS

Jan Söderkvist
Colibri Pro Development AB
Täby, Sweden

ABSTRACT

Simulations can be performed either analytically or numerically. A comparison between the two approaches for a simple demonstrator case, a piezoelectric cantilever beam, is made. Various parameters are used to validate the piezoelectric capabilities of ANSYS. For example, FEA predicts accurately static deflections, harmonic response, and the crystal impedance as a function of frequency. It is shown that FEA can be used either separately, or in combination with the analytic approach. This enables the transfer of the three-dimensional piezoelectric problem for beams into a numerical two-dimensional dielectric and a one-dimensional mechanical problem. The results have been successfully compared with experiments.

1. INTRODUCTION

Piezoelectric materials are used in many energy actuators, resonators and sensors (Pointon 1982). Piezoceramics (PZT, ...) (Gallego-Juárez 1989, Smith 1992) and piezoelectric polymers (PVDF, ...) (Marcus 1981, Chen and Payne 1995) are often used in ultrasonic applications and in simple loudspeakers, e.g. in buzzers. Crystalline piezoelectric materials (SiO_2, $LiNbO_3$, GaAs,...) are more often used in resonators and precision sensors (Studer and Zingg 1990, Danel and Delapierre 1991). Thin films of piezoelectric materials (ZnO, AlN, ...) can be added to the surface of small structures to excite or detect mechanical vibrations (Kunisch and Holleck 1995). Bending modes of beams and plates are normally used for kHz-resonators and for actuators. Thickness shear modes of plates are commonly used for MHz-resonators.

The use of piezoceramics and piezoelectric polymers in actuators is motivated by their high efficiency in converting electrical energy into mechanical energy. However, the high value of the piezoelectric coupling coefficients leads to non-negligible dependencies of performance parameters on the piezoelectric effect. For instance, mechanical resonance frequencies and the measured "dielectric" capacitance can increase substantially due to this. For piezoceramics, simulations are often used to optimize the energy conversion under various conditions.

Quartz is the most frequently used crystalline piezoelectric material. Its chemical inertness (⇒ low aging) and strong

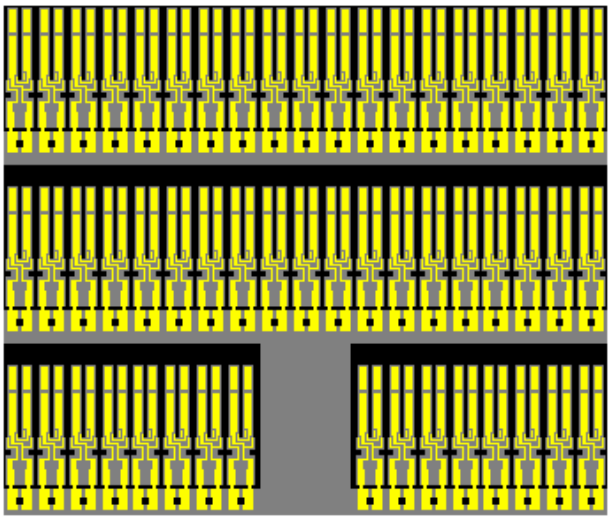

FIGURE 1. Part of a watch crystal wafer. The tuning forks are produced by etching 100-200 μm thick quartz wafers. Wafer processing and micromachining make the production economically feasible. Internationally, more than 100,000 watch crystals are manufactured each hour.

anisotropy (⇔ low temperature dependence of the frequency) makes it an excellent material for resonators. In fact, every computer and mobile phone, and most watches, contains quartz resonators (Figure 1). The extreme stability of quartz resonators is well illustrated by some microprocessor compensated crystal oscillators (MCXOs) that have a frequency error over full temperature range, including one year of aging, of less than one second per year (0.03 ppm) (Benjaminson and Stallings 1989). To take full advantage of the excellent properties of quartz, a proper selection of vibration mode(s) and design of the geometry is essential. Simulations are here more aimed at reducing error sources and to obtain a stable "working point."

Piezoelectric materials are used also in sensors (EerNisse *et al* 1988, Söderkvist 1994, Benes *et al* 1995). Highest accuracy is obtained for resonating sensors made from crystalline materials. For instance, quartz sensors with a dynamic range as high as 10^7-10^8 exist (Meldrum 1990). To obtain this performance, simulations are very helpful in the design phase and in creating an understanding for the functioning of the device.

Clearly, the requirements for the various applications differ. For piezoceramics, a large amplitude is often needed; for crystalline materials, the stability of the frequency is essential. Nevertheless, for all applications and materials, it is desirable that the design of the active part is well optimized. Since piezoelectric parts often are key elements of a device, it is necessary to be able to understand and predict their functioning.

Finite element analysis for predicting the performance of piezoelectric structures is treated in this article. Of special interest is to determine if FEA accurately can predict the piezoelectric contribution to the electric and mechanical properties.

Quartz and PZT cantilever beams are used as test geometries due to the difficulty to treat the piezo-electro-mechanical interaction analytically for other geometries. The FEA results are most easily compared with analytic expressions for bending

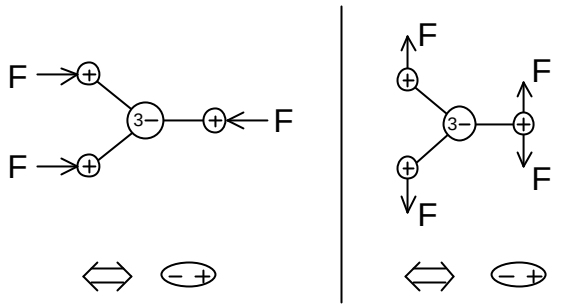

FIGURE 2. Dipoles generated by forces acting on a schematic crystal unit. The orientation of the dipoles generated by the two illustrated force-directions are identical. This shows one aspect of the anisotropy of the piezoelectric effect.

modes of beams. If the agreement is satisfactory for beams, it can be assumed that FEA can be used accurately also for more complicated geometries. Tests have been carried out successfully also for shear vibrations.

2. PIEZOELECTRICITY

A general background of the piezoelectric effect is given below, although most of you are already familiar with it. The background is used to point out certain characteristics of piezoelectricity that will be addressed in the following.

The piezoelectric conversion of mechanical into electrical energy (and vice versa) is due to the generation of atomic dipoles within the material. Figure 2 shows that the deformation-induced electric response often can have a direction different from the applied force. This anisotropic effect must be accounted for if the material is to be modeled accurately. One consequence is that the material parameters should be given in matrix form, as indicated in the Appendix 1. In this appendix, the difference between the two

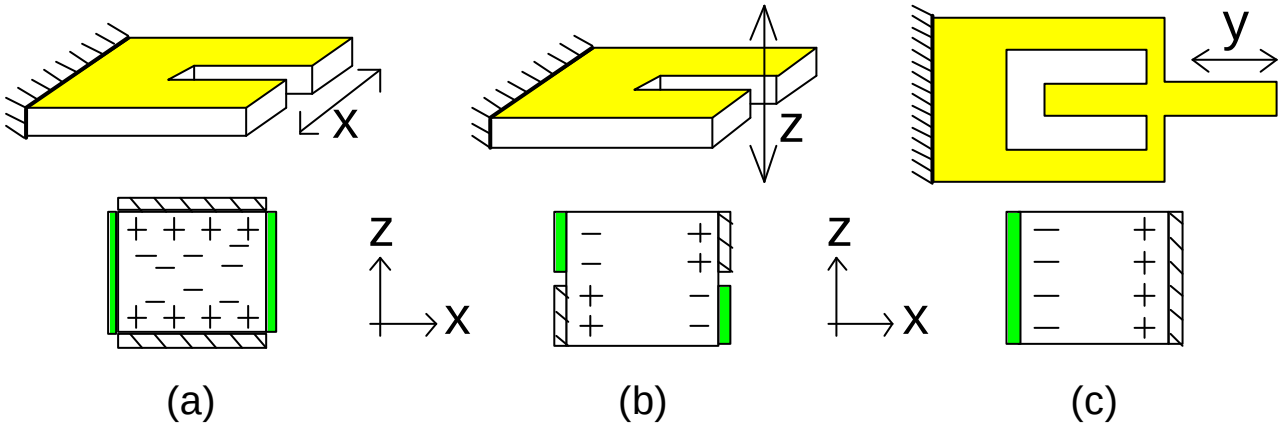

FIGURE 3. Piezoelectrically generated bound charges for PZT and GaAs (a) and quartz (b,c) for three common low-frequency vibrations. Included in the lower part of the figure is the best electrode configuration for each charge distribution and cross-section.

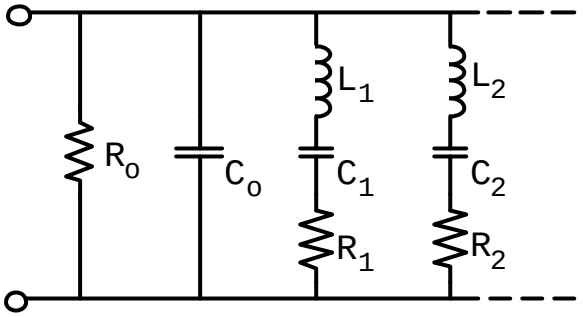

FIGURE 4. An electric equivalent circuit for piezo electric resonators. The $R_nC_nL_n$ branches represent the mechanical behavior close to the nth resonance frequency, and R_o and C_o the resistive and dielectric behavior. Note that L_n, C_n and R_n represent the mechanical kinetic, potential and loss energies, respectively.

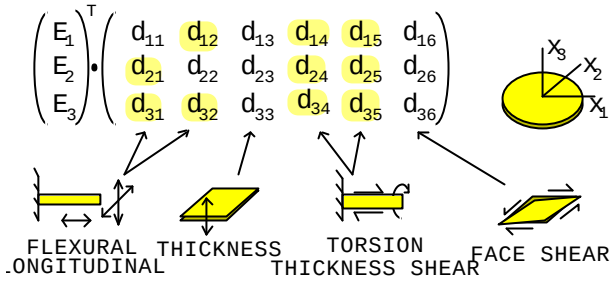

FIGURE 5. Suitable coefficients in the d_{ik}-matrix for activating various vibration modes. Each row represents one direction of the electric field and each column a mechanical stress component.

commonly used ways of arranging the parameters is illustrated.

The deflection-induced dipoles are easiest interpreted if they are represented with bound volume and surface charges (Figure 3). The bound charges try to attract free charges, preferably to the electrodes. This will be observed as a detectable current. For a material with a finite resistivity, the bound charges can be neutralized by free charges within the material (Söderkvist 1995). This is undesirable since it reduces the amount of free charges attracted to the electrodes, and it explains why most piezoelectric materials are dielectric (negligible leak-currents). The calculation is by that simplified noticeably also when numerical methods are used.

An electric field applied to a piezoelectric material may pull the dipoles so that a mechanical deformation arises. The resulting mechanical force is instantaneously proportional to the applied field, unless its frequency is so high that electromagnetic theory has to be used to describe the field. In the following, it will be assumed that the electric fields can be treated electrostatically.

Mechanical resonance frequencies, such as those in Figure 3, can be excited by time-varying the field. The resonance frequencies are experimentally found by noting that the amount of piezoelectrically generated charges is proportion to the mechanical deformation. At resonance, this results in a rapid increase in magnitude and a rapid change in phase of the piezoelectrically generated current. It is possible to represent this behavior with a two-port equivalent circuit (Figure 4). The voltage represents the force and the current through the $R_nC_nL_n$ branches the mechanical velocity decomposed into the mechanical eigenmodes. Mechanical resonance frequencies can be found electrically by observing the phase of the impedance. FEA-determined values of the equivalent components in Figure 4 can be compared with measured values.

The equivalent circuit reveals that the piezoelectric effect is best suited for resonators and dynamic measurements. Static deflections can more easily be studied with FEA then in reality due to FEA not being dependent on high quality charge amplifiers with very low leak currents.

The design of a piezoelectric device is strongly facilitated if the location of the piezoelectrically generated charges is known. For instance, this increases the understanding of how the electrodes should be optimized. Therefore, the determination of the piezoelectrically induced bound charges is a key factor.

The piezoelectrically generated charges create an electric field, $\boldsymbol{E}^p$, that is superimposed on that due to the voltage applied to the electrodes, $\boldsymbol{E}^d$. Its orientation is such that it reduces the effect of $\boldsymbol{E}^d$. $\boldsymbol{E}^p$ also generates a force that tries to prevent deflections. This results in an increased stiffness of the material with, for example, a resulting increase in mechanical resonance frequency. The effect can be substantial for materials with a strong piezoelectric effect. A complication is that the magnitude and shape of $\boldsymbol{E}^p$ depends on the location of the electrodes and if the electrodes are electrically connected. Nevertheless, the effect can be negligible even for strongly piezoelectric materials, if the electrodes are located where the bound surface charges are generated and if no bound volume charges are generated.

The relation between an applied electric field and resulting mechanical deflection is given by the piezoelectric constant matrix, d_{ik}. Whether a certain mechanical vibration can be excited piezoelectrically is controlled by the non-zero components in the piezoelectric d_{ik}-matrix (Figure 5). An undesired zero-value of a d_{ik}-component can be overcome by rotating the geometry relative the crystallographic structure. FEA is well adapted for testing the effect of such rotations on, for instance, the temperature dependence of resonance frequencies, and the suppression of undesired vibration modes.

3. ANALYTIC APPROACH

The ideal solution would be if an analytic approach could be used. A deeper understanding can be gained from studying and manipulating analytic expressions. However, despite the advantage of this method, it is not commonly used for several reasons. For instance, a deep knowledge of the piezoelectric phenomena is needed to set up the basic equations correctly, the

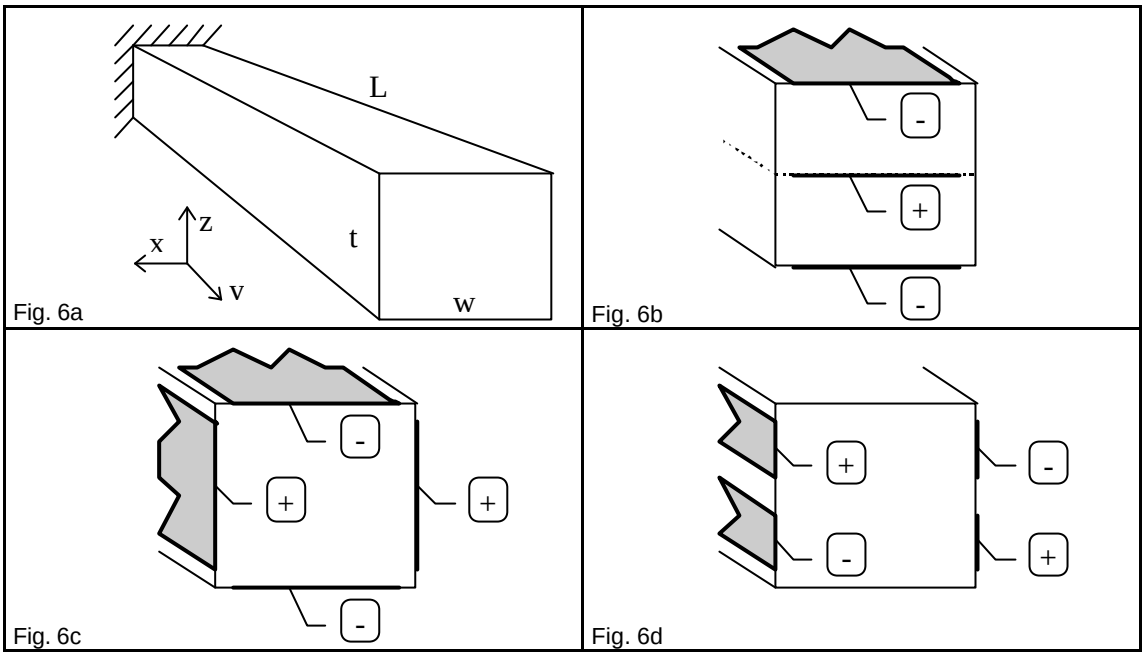

FIGURE 6. Basic geometry of the cantilever beam. Included are three electrode configurations with polarities of the applied voltage. Configuration 6b is used for piezoceramic bimorphs poled in the z-direction (z-vibrations), 6c for piezoceramics (z-vibration) and quartz (x-vibration), and 6d for piezoceramics (x-vibration) and quartz (z-vibration).

approach can only be used on a limited number of geometries, and approximations are often needed for this approach to be manageable.

The finite element analysis overcomes most of these drawbacks, but has the disadvantage that the understanding is restrained by the lack of analytic expressions. Nevertheless, simulations are very useful for studying the piezoelectric effect. The following will show that FEA and the analytic approach gives comparable results also for the piezoelectric effect.

Bending cantilever beams are used as the illustrating example since the analytic approach is fairly straight forward. Length expanding beams are easier to handle analytically, but are less general for validating the FEA approach. Using a more complicated geometry would take away the focus of this article on piezoelectric FEA simulations.

Assume that the electrodes are located such that no electric field components in the length direction of the beam are intentionally introduced. Then, in a first approximation, the electric field in the direction of the beam in Figure 6 can be neglected, and the electric problem becomes two-dimensional. Assume also that ordinary beam theory can be used to describe the mechanical system. This transfers the mechanical problem into being one-dimensional with a piezoelectric force acting on it. It can be shown that the differential equation describing the bending deflection in the xy-plane, $z_x(y)$, is given by (Söderkvist 1991a):

$$\rho A \cdot \frac{\partial^2 \varsigma_x(y)}{\partial t^2} + 2\delta \cdot \frac{\partial \varsigma_x(y)}{\partial t} + \frac{\partial^2}{\partial y^2}\left(\frac{I_z}{s_{22}} \cdot \left(1 - \int_p\right) \frac{\partial^2 \varsigma_x(y)}{\partial y^2} \right) = f(y) - \frac{\partial^2 \int_d}{\partial y^2} \quad (1)$$

where ρ, A, δ, I_z, s_{22}, and $f(y)$ are the density, cross-section area, damp factor, second moment of area with respect to the z-axis, compliance in the direction of the beam (s_{22}=1/Young's modulus), and a distributed force, respectively.

The integrals $\int_d$ and $\int_p$ are two parameters that depend on the piezoelectric field and the electrode configuration. The piezoelectric force is represented by $\int_d$, and the change in stiffness due to the piezoelectric effect by $\int_p$. For the bending in the xy-plane, $\int_d$ and $\int_p$ equal:

$$\int_d = \int \frac{x \cdot d_{i2}}{s_{22}} E_i^d \, dx dz \quad (2a)$$

$$\int_p = \int \frac{x \cdot d_{i2}}{I_z} U_i^p \, dx dz \quad (2b)$$

where x is the distance from the bending center. The integrals in eq. (2) are to be taken over the cross-section area. The index $_i$

Table 1	PZT			quartz	
Analytic approach	Fig. 6b	Fig. 6c	Fig. 6d	Fig. 6c	Fig. 6d
$\delta_d = DVw^2/2s_{22}$ ®	d_{32}	d_{32}	d_{32} 0.32	d_{12}	d_{12} 0.5
δ_p	$-k_{32}^2$ 0.25	$-k_{32}^2$ 0.42	$-k_{32}^2$ 0.23	$-k_{12}^2$ 0.42	0
f_1(with piezo) [kHz]	17.96	18.12	18.95	29.33	29.26
Static deflection at tip of beam [nm/volt]	36.9	35.3	11.4	0.687	0.345
C_o (no piezo) [pF]	138.1	∞ (infinitely small distance between electrodes)			
C_1 [pF]	6.8	6.5	0.66	0.0023	0.00057

TABLE 1. Some results for the analytic approach for the electrode configuration in Figure 6.

indicates the piezoelectrically useful component of the electric field. The strain-induced piezoelectric field $\boldsymbol{U}^p$ is normalized via $\boldsymbol{E}^p = -\boldsymbol{U}^p \cdot \partial^2\zeta/\partial y^2$, i.e. via the local curvature of the beam. This makes δ_p independent of the applied voltage while δ_d is proportional to the applied voltage.

A consequence of δ_p is that the mechanical resonance frequency increases in an electrode configuration dependent way due the piezoelectric effect by (cf. eq. (1)):

$$f_n(\text{with piezo}) = f_n(\text{no piezo}) \cdot \sqrt{1-\int_p} \tag{3}$$

where $$f_1(\text{no piezo}) = \frac{w \cdot 0.162}{L^2\sqrt{r \cdot s_{22}}}$$

and f_n is the n^{th} resonance frequency, and f_1 the fundamental resonance frequency for a cantilever beam of width w (x-direction) and length L (Young 1989). It can be shown that $0 \le -\delta_p \le k_{i2}^2$, where k_{i2} is the piezoelectric coupling coefficient for the studied vibration ($k_{i2}^2 = d_{i2}^2/s_{22}e_{ii}$). For complicated electric fields, k_{i2} should be replaced with an effective value of the piezoelectric coupling coefficient. Equation (3) means that the change in frequency can be substantial, but it can also be negligible for some electrode configurations (see Table 1).

Similarly, the electric behavior is also affected. A piezoelectric contribution is added to the dielectric capacitance, C_o, as indicated in Figure 4. At frequencies well below the fundamental resonance frequency, one measures the capacitance:

$$C(\text{low frequency}) = C_o + \sum_{n=1}^{\infty} C_n \approx C_o \cdot \left(1 + k_{i2}^2\right) \tag{4}$$

The last part of eq. (4) is due to k_{i2}^2 being defined via the piezoelectric electro-mechanical energy conversion. The piezoelectric energy will be distributed among the $R_nC_nL_n$-branches in Figure 4, which means that the value of each C_n in Figure 4 will be smaller than $k_{ik}^2 \cdot C_o$.

From eq. (1), one can easily derive the static deflection via the local curvature of the beam. Assume that no external force acts on the beam. This gives:

$$\frac{\partial^2 V_x(y)\big|_{static}}{\partial y^2} = -\int_d \cdot \frac{s_{22}}{I_z \cdot \left(1-\int_p\right)} \tag{5}$$

where the integral δ_d equals zero in the un-electrode covered regions. Integrating eq. (5) twice and adopting the solution to the boundary conditions gives the static deflection. Equation (5) can easily be used for beams with varying cross-section dimensions and material parameters, and to study the dependence of the deflection on the electrode location.

The dynamic amplitude at frequency f can be obtained by solving eq. (1) and treating the piezoelectric force as a generalized force, or by decomposing the static deflection or the piezoelectric force into the mechanical eigenmodes, $\xi_n(y)$. The second approach gives:

$$V_x(y)\big|_{dynamic} = \sum_n \frac{\Phi_n}{m_n} \cdot \frac{x_n(y) \cdot \sin(2\pi ft + \varphi_n)}{4\pi^2 \cdot \sqrt{\left(f_n^2 - f^2\right)^2 + \left(\frac{f \cdot f_n}{Q_n}\right)^2}} \tag{6a}$$

where Q_n is the Q-value ($Q_n = \pi f_n/\delta$), m_n a generalized mass ($m_n = \int x_n(y)^2 r A dy$), and φ_n a phase angle ($\varphi_n = \tan^{-1}[ff_n/(Q_n(f_n^2 - f^2))]$) for the n^{th} eigenmode. Equation (6a) is closely related to the equivalent circuit in Figure 4. Each term in eq. (6a) is corresponds to an $R_nC_nL_n$-branch in Figure 4. The decomposition constants F_n are given by:

$$\Phi_n = -\int\left(\int_d \cdot \frac{\partial^2 \xi_n(y)}{\partial y^2}\right)dy \qquad (6b)$$
$$= \left(2\pi f_n\right)^2 \cdot \int\left(\zeta_x(y)\big|_{static} \cdot \xi_n(y)\right)\rho A dy$$

where the first expression is obtained by an eigenmode-decomposition of the force and the second of the static deflection.

The electrode current generated by a mechanical deflection is given by (Söderkvist 1990):

$$I_p = \oint \dot{D}^p \, dA_{electrode}$$
$$= j2\pi f \int\left(\frac{\partial^2 \zeta(y)\big|_{dynamic}}{\partial y^2} \cdot \frac{\int_d}{\Delta V}\right)dy \qquad (7)$$

where $\boldsymbol{D}$ is the electric displacement vector and DV the applied voltage. The values of the equivalent components can be found by determining the current for each term in eq. (6a). This gives:

$$C_n = \frac{\Phi_n^2}{\left(2pf_n \cdot \Delta V\right)^2 m_n} \qquad (8)$$

The other equivalent components are given by $(2\pi f_n)^2 L_n C_n = 1 = (2\pi f_n) R_n C_n Q_n$. Corresponding expressions can be derived for torsional and longitudinal vibrations (Söderkvist 1991b).

The key to the analytic approach is to determine the values of the integrals ϑ_d and ϑ_p. Analytically, this can be very tedious for arbitrary electrode configurations. Best is if the sides of the cross-section either are fully electrode covered or do not have any electrodes at all. Even if this condition is fulfilled, it may be a tedious task unless the field can be treated one-dimensionally. For example, the analytic expressions for $\boldsymbol{E}^d$ and $\boldsymbol{E}^p$ for the electrode configuration in Figure 6b are very simple, while those for the configuration in Figure 6c are given by an infinite sum of trigonometric and hyperbolic functions.

Assume that the electrodes go all the way out to the edges of the cross-section and that they cover the entire length of the beam. This results in the expressions and values in Table 1 for a $3\times0.3\times0.3$ mm^3 beam ($w=t$) with electrodes according to Figure 6.

4. ANALYTIC-FEA APPROACH

As pointed out, the key to the analytic approach are the integrals ϑ_d and ϑ_p. The tediousness of the analytic approach can be relaxed substantially by determining them numerically. The numerically determined ϑ_d and ϑ_p can be used in the remaining analytic expressions. This combines the best from the analytic and the numerical approaches. A good general understanding can be retained while more general electrode configurations can be studied.

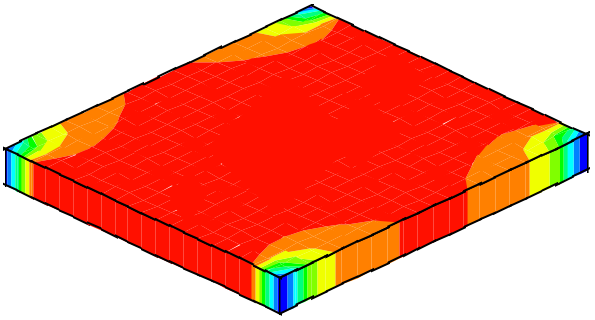

FIGURE 7. Piezoelectric field intensity in the cross-section of a beam for the electrode configuration in Figure 6c. The figure represents the integrand of ϑ_d. Carrying out the integration (summing over the elements) will result in a non-zero value of ϑ_d for this electrode configuration and vibration direction.

Finite element analysis is well suited for determining the values of ϑ_d and ϑ_p. Equation (2) shows that the determination of ϑ_d can be based on the dielectric part of the electric field. This means that any FEA program that can handle two-dimensional electrostatic problems (or thermal problems) can be used to determine ϑ_d via the dielectric field $\boldsymbol{E}^d$. The integration in eq. (2) can be carried out outside the FEA program, once $\boldsymbol{E}^d$ is known.

The FEA program ANSYS has the advantage that the postprocessing capabilities are advanced. This enables the evaluation of the integral in eq. (2) to be carried out without leaving ANSYS. Storing the components that are to be integrated with the ETABLE command and using the SMULT and SSUM commands performs the task (Figure 7). A simple *GET command makes it possible to retrieve and store the result.

The FEA-analytic approach is suitable for automation. One FEA-model of the cross-section can be used for studying different electrode configurations by just changing the electric boundary conditions. Electrodes that are not connected to the outside world can be included by using the CP command to couple the nodes that represent such electrodes, and by not applying a voltage boundary condition to the coupled sets. Symbolic mathematics programs, like MatcCad, Maple and Macsyma, can be used to evaluate the analytic expressions once the FEA determined values of the integrals are known.

The value of ϑ_d can also be found via the piezoelectric part of the electric field. This gives an option of treating the problem either dielectrically or purely piezoelectrically. It can be shown that ϑ_d equals $DV \cdot r_p \cdot k_{fraction}/(\partial^2 z/\partial y^2)$ where r_p denotes the amount of piezoelectrically generated bound positive charge in the cross-section. The constant $k_{fraction}$ is the ratio between the charge that appears at the positive electrodes and r_p. This method of determining ϑ_d is best suited for understanding how different electrode configurations work. However, it is less suited for determining the value of ϑ_d.

Table 2 Analytic-FEA approach	PZT			quartz	
	Fig. 6b	Fig. 6c	Fig. 6d	Fig. 6c	Fig. 6d
$\int_d$ (FEA via $\boldsymbol{E}^d$) [Nm]	$4.50 \cdot 10^{-7}$	$4.57 \cdot 10^{-7}$	$1.43 \cdot 10^{-7}$	$8.17 \cdot 10^{-9}$	$4.07 \cdot 10^{-9}$
$\int_d$ (analytically) [Nm]	$4.50 \cdot 10^{-7}$	$4.50 \cdot 10^{-7}$	$1.42 \cdot 10^{-7}$	$8.10 \cdot 10^{-9}$	$4.05 \cdot 10^{-9}$
$k_{fraction}$ (FEA via $\mathbf{E}^p$)	50.0 %	52.3 %	63.8 %	50.5 %	100 %
$k_{fraction}$ (analytically)	50 %	50 %	63.2 %	50 %	100 %
$\int_p$ (FEA via $\mathbf{E}^p$)	-0.025	-0.042	-0.023	-0.0043	0
$\int_p$ (analytic expression)	-0.027	-0.045	-0.025	-0.0044	0

TABLE 2. Numerically determined values of the integrals $\int_d$ and $\int_p$ for the electrode configurations in Table 1 and a 1 volt excitation voltage. The results are compared with the analytic expressions.

The location of the bound volume and surface charges is given by:

$$\begin{cases} \mathbf{P} = \mathbf{d} \bullet \mathbf{T} \\ r_{vol} = -div\mathbf{P} \\ r_{surf} = \mathbf{P} \bullet \mathbf{n}_{out} \end{cases} \tag{9}$$

where $\boldsymbol{n}_{out}$ is the normal out of the material and $\boldsymbol{P}$ is the piezoelectric polarization for a local mechanical stress, $\boldsymbol{T}$. For a bending beam, $\boldsymbol{T}$ equals $u \cdot (\partial^2 z / \partial y^2) / s_{22}$ where u denotes the distance in the direction of vibration from the bending center. The second derivative that is included in the equations on this page disappears when $\int_d$ is determined. Therefore, for simplicity, set $\partial^2 z / \partial y^2$ equal to 1 in the calculations. In Figure 6, configurations 6b and 6c (r_p(PZT)=$wt \cdot d_{32}/s_{22}$, r_p(quartz)=$wt \cdot d_{12}/s_{22}$) has a uniform distribution of volume charges, and configuration 6d (r_p(PZT)=$w^2 \cdot d_{32}/4s_{22}$, r_p(quartz)=$t^2 \cdot d_{12}/4s_{22}$) has no volume charges. For PZT, the surface charges are located on the z-surfaces, and for quartz, on the x-surfaces.

The value of $\int_p$ is also based on the piezoelectric part $\boldsymbol{E}^p$ of the electric field. Its value can be determined in the same way as $\int_p$. Note that the electrodes should be short-circuited during simulations that are based on $\boldsymbol{E}^p$. This prevents the introduction of the dielectric field.

The FEA determined values for the configurations in Table 1 are listed in Table 2. The simulations are based on a thermal model (PLANE77, $V \leftrightarrow$T, $e_{11} \leftrightarrow k_{xx}$, etc.) with a 40×40 elements mesh. The simulations could equally well be based on an electrostatic element, such as PLANE121. The thermal element was chosen to illustrate that the piezoelectric analysis can be carried out also with finite element programs that do not have electrostatic and piezoelectric capabilities. The volume charges ($-d_{32}/s_{22}$ [PZT, z-vib.], $-d_{12}/s_{22}$ [quartz, x-vib.]) were added via the BF,ALL,HGEN command, and the surface charges ($td_{32}/2s_{22}$ [PZT, z-vib., z-surf.], xd_{32}/s_{22} [PZT, x-vib., z-surf.], $wd_{12}/2s_{22}$ [quartz, x-vib., x-surf.], zd_{12}/s_{22} [quartz, z-vib., x-surf.]) via the SFL,#,HFLUX and SBCTRAN commands. The bound charges at the electrodes must be added separately during the postprocessing phase when $k_{fraction}$ is determined.

The deviation between the analytic approach and the FEA results are mostly due to the analytic approach using an isotropic value of the permittivity $\boldsymbol{e}$. Repeating the FEA simulations using the isotropic value used in the analytic approach reduces the deviation to below 0.5 %.

The conclusion is that simulations can be used successfully together with the analytic approach. This facilitates, for instance, the inclusion of anisotropic material parameters, and gives a possibility to test a large number of electrode configurations in a time-efficient way.

5. FEA APPROACH

One drawback with the analytic(-FEA) approach is that electric field components in the direction of the beam are neglected. Describing the beam with isotropic classical one-dimensional beam theory can also introduce errors. A third limitation is that the effect of only a few of the material constants is considered.

In many cases, it is of interest to treat the electric field and the mechanical problem three-dimensionally. If not before, a three-dimensional model should be used to test the validity of other design approaches used. Such a model could reveal odd effects, for instance that a quartz beam that is pulled may start to twist due to the non-zero value of s_{14}. Such effects are difficult to predict correctly without using an anisotropic three-dimensional piezoelectric model. The simulations show that small errors can be expected if "unimportant" material parameters are neglected, as in the analytic approach.

Some finite element programs, like ANSYS, can handle piezoelectric materials and their anisotropic material properties. These programs can be used to determine, for example, the

Table 3	analytic		3D-FEA		
Fig. 6b, PZT	all d_{ik}=0	only $d_{32}\neq 0$	all d_{ik}=0	only $d_{32}\neq 0$	all d_{ik} active
d_s [nm/volt]	0	36.0	0	36.1	34.6
d_d [μm/volt]	0	16.4	0	16.5	15.5
$d_d/(d_s \cdot Q)$	N.A.	0.89	N.A.	0.91	0.90
$\grave{o}_d$ (eq. 5) [Nm]	0	$4.50 \cdot 10^{-7}$	0	$4.50 \cdot 10^{-7}$	$4.30 \cdot 10^{-7}$
$\grave{o}_p$ (eq. 3)	0	-0.0267	0	-0.0223	-0.0178
f_1 [kHz]	17.73	17.96	17.90	18.10	18.06
Q	N.A.	500	N.A.	511	508
R_1 [kΩ]	∞	2.50	∞	2.52	2.83
C_1 [pF]	0	7.0	0	6.8	6.1
$C_o + \sum C_n$ [pF]	138.1	153	138	159	194
k_{eff} (eq. 4) [%]	0	33	0	39	64

TABLE 3. FEA determined values for PZT, the electrode configuration in Figue 6b, and a 1 volt excitation voltage.

Table 4	analytic		3D-FEA		
Fig. 6c, PZT	all d_{ik}=0	only $d_{32}\neq 0$	all d_{ik}=0	only $d_{32}\neq 0$	all d_{ik} active
d_s [nm/volt]	0	35.3	0	29.4	30.9
d_d [μm/volt]	0	15.7	0	13.7	13.9
$d_d/(d_s \cdot Q)$	N.A.	0.89	N.A.	0.93	0.90
$\grave{o}_d$ (eq. 5) [Nm]	0	$4.5 \cdot 10^{-7}$	0	$3.7 \cdot 10^{-7}$	$3.9 \cdot 10^{-7}$
$\grave{o}_p$ (eq. 3)	0	-0.0451	0	-0.0387	-0.0269
f_1 [kHz]	17.73	18.12	17.91	18.25	18.15
Q	N.A.	500	N.A.	512	512
R_1 [kΩ]	∞	2.71	∞	3.63	3.50
C_1 [pF]	0	6.5	0	4.7	4.9

TABLE 4. FEA determined values for PZT, the electrode configuration in Figue 6c, and a 1 volt excitation voltage.

piezoelectric response, the equivalent impedance, and the piezoelectrically caused electrode dependent change of the resonance frequencies. The three-dimensional FEA approach can be used with a smaller amount of knowledge about the piezoelectric effect, and does not rely on analytic approximations made by the user. Thus, it can be assumed that the FEA approach results in better agreement with reality than the analytic approach.

In the following, a three-dimensional FEA model is used to study the electrode configurations in Table 1. The model is based on the multi-field element SOLID5 with the anisotropic stiffness and the piezoelectric material parameters input as c_{ik} and e_{ik} with the TBDATA command. The matrix inversion of s_{ik} and d_{ik} in Appendix 1 was carried out using MathCad to avoid numerical errors. Millimeter was used as the length unit instead of the natural choice, μm. An undesired consequence of using μm is that the voltage exceeds the displacement limit of ANSYS due to the voltage being scaled as length^{-2}.

The simulations for each electrode configuration started with a static analysis with a voltage applied to the electrodes. The main purpose of this simulation was to determine if the deflection was in the expected regime, and thus if the FEA and analytic models were in agreement. Second, a modal analysis was carried out to locate the fundamental resonance frequency. This information was

Table 5	analytic		3D-FEA		
Fig. 6d, PZT	all d_{ik}=0	only $d_{32}\neq 0$	all d_{ik}=0	only $d_{32}\neq 0$	all d_{ik} active
d_s [nm/volt]	0	11.4	0	11.6	11.6
d_d [μm/volt]	0	5.12	0	5.27	5.19
$d_d/(d_s \cdot Q)$	N.A.	0.89	N.A.	0.91	0.89
$\grave{o}_d$ (eq. 5) [Nm]	0	$1.42 \cdot 10^{-7}$	0	$1.44 \cdot 10^{-7}$	$1.43 \cdot 10^{-7}$
$\grave{o}_p$ (eq. 3)	0	-0.0249	0	-0.0202	-0.0134
f_1 [kHz]	17.73	17.95	17.91	18.09	18.03
Q	N.A.	500	N.A.	510	507
R_1 [kΩ]	∞	26.7	∞	24.6	25.4
C_1 [pF]	0	0.66	0	0.70	0.69

TABLE 5. FEA determined values for PZT, the electrode configuration in Figue 6d, and a 1 volt excitation voltage.

Table 6	analytic		3D-FEA		
Fig. 6c, quartz	all d_{ik}=0	only $d_{12}\neq 0$	all d_{ik}=0	only $d_{12}\neq 0$	all d_{ik} active
d_s [nm/volt]	0	0.69	0	0.74	0.86
d_d [μm/volt]	0	6.12	0	6.48	7.35
$d_d/(d_s \cdot Q)$	N.A.	0.89	N.A.	0.88	0.85
$\grave{o}_d$ (eq. 5) [Nm]	0	$8.1 \cdot 10^{-9}$	0	$8.7 \cdot 10^{-9}$	$10.1 \cdot 10^{-9}$
$\grave{o}_p$ (eq. 3)	0	-0.00439	0	-0.000478	-0.00060
f_1 [kHz]	29.26	29.33	29.17	29.17	29.17
Q	N.A.	10,000	N.A.	9,960	9,950
R_1 [kΩ]	∞	240	∞	215	167
C_1 [fF]	0	2.26	0	2.55	3.28

TABLE 6. FEA determined values for quartz, the electrode configuration in Figue 6c, and a 1 volt excitation voltage.

used to determine the starting and ending frequencies for a harmonic analysis in which the behavior near resonance was studied. In addition, the low-frequency (dielectric) capacitance was determined for the PZT-bimorph.

The results of the simulations are summarized in Tables 3 to 7. The parameters were derived as follows:

- *Static deflection, d_s, at the tip of the tine:* The static simulation gives the FEA result, and eqs. (2) and (5) the analytic result.
- *Dynamic deflection, d_d, of the fundamental eigenmode at resonance:* The FEA-determined amplitude equals the maximum of the imaginary part of the displacement of the beam tip during the harmonic simulation. Using the imaginary part gives a possibility to suppress the amplitude contribution from other eigenmodes due to the 90° phase shift between the applied force (voltage) and the resulting deflection at resonance (cf. j_n in eq. (6a)). The analytic result is obtained from eq. (6). See Figure 8a.
- *Dynamic amplification factor $d_d/(d_s \cdot Q)$:* This number indicates how well the deflection shape of the static deflection agrees with that of the fundamental eigenmode. Equation (6b) gives the analytic result directly if the eigenmode is normalized to unit deflection at the tip.
- $\grave{o}_d$*:* For FEA, this parameter is determined from the static amplitude and eq. (5). For the analytic approach, eq. (2) is

Table 7 Fig. 6d, quartz	analytic		3D-FEA		
	all d_{ik}=0	only $d_{12}\neq 0$	all d_{ik}=0	only $d_{12}\neq 0$	all d_{ik} active
d_s [nm/volt]	0	0.34	0	0.35	0.39
d_d [µm/volt]	0	3.07	0	3.10	3.49
$d_d/(d_s \cdot Q)$	N.A.	0.89	N.A.	0.88	0.89
$\grave{o}_d$ (eq. 5) [Nm]	0	$4.1\cdot10^{-9}$	0	$4.2\cdot10^{-9}$	$4.6\cdot10^{-9}$
$\grave{o}_p$ (eq. 3)	0	0	0	0	0
f_1 [kHz]	29.26	29.26	29.23	29.23	29.23
Q	N.A.	10,000	N.A.	9,960	9,950
R_1 [kΩ]	∞	955	∞	934	736
C_1 [fF]	0	0.569	0	0.585	0.743

TABLE 7. FEA determined values for quartz, the electrode configuration in Figue 6d, and a 1 volt excitation voltage.

used.

- $\grave{o}_p$*:* Determined from FEA simulations by comparing the resonance frequencies with and without the piezoelectric material parameters active, via eq. (3). Equation (2) gives the analytic result.
- f_1*:* The resonance frequency is defined as the frequency at which the imaginary part of the dynamic deflection has its maximum. This frequency is very close, but not equal, to that found via the modal analysis. Equation (3) gives the analytic result.
- Q*:* The FEA-determined Q-value is obtained by measuring the width of the conductance curve, i.e. the real part of the admittance, at the conductance value $1/2R_1$. The admittance is found by multiplying the charge collected at the electrodes with $2\pi f_1$. This can be done in ANSYS by using the CP, RFORCE and PROD commands in POST26. The ratio between the resonance frequency and this peak width equals Q. The analytic number is the value used as input for the simulations.
- R_1*:* The maximum of the conductance equals the resistive part

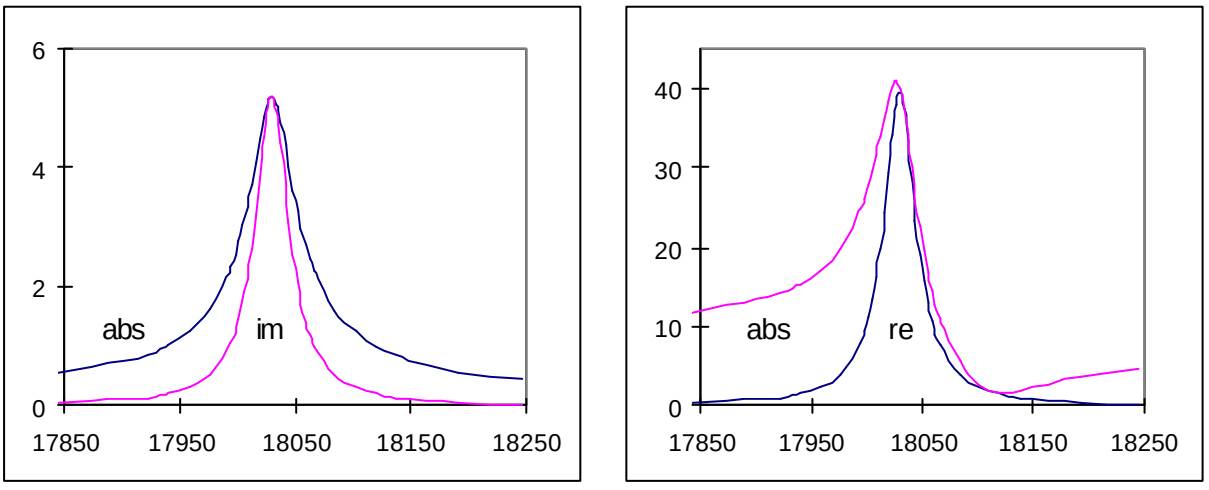

(8a) (8b)

FIGURE 8. Two results from the harmonic FEA-simulations on the electrode configuration in Figure 6d (PZT): a) the absolute value and the imaginary part of the mechancial deflection [µm], and b) the absolute value and the real part of the admittance [µS], plotted as a function of frequency [Hz].

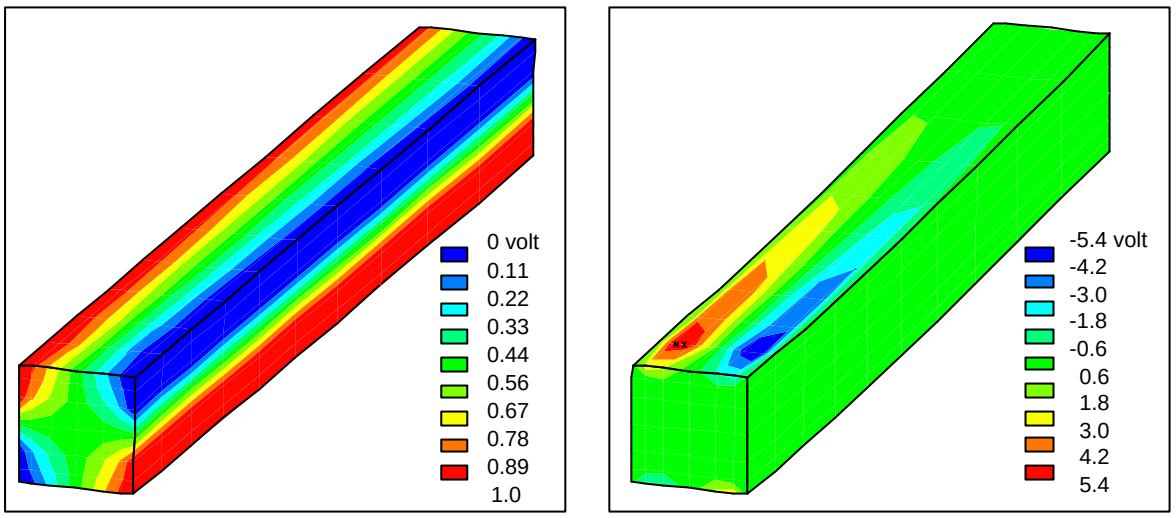

(9a) (9b)

FIGURE 9. The electric voltage in the cross-section of the beam at resonance for the electrode configuration in Figure 6d (PZT). The figure to the left shows the situation when the harmonic voltage reaches its maximum, and that to the right when the voltage passes zero. The beam is clamped at the lower-left cross-section.

of the crystal impedance in Figure 4. Using the conductance makes it possible to distinguish the resonance branches in Figure 4 from the dielectric branch (C_o), as shown in Figure 8b. The analytic value of R_1 is found via eq. (8) and the expression given right below this equation.

- C_1: Determined from R_1 and Q, and from eq. (8) respectively.
- $C_o + \sum C_n$: The low frequency capacitance equals the charge collected at the electrodes for the static simulation for a 1 volt excitation voltage. The analytic value is set equal to that for a plate capacitor multiplied by $1+k^2$. The calculation of the dielectric capacitance was not carried out for the electrode configurations in Figures 6c and 6d since the analytic approach, to which the values should have been compared, results in an infinite dielectric capacitance.
- k_{eff}: A rough approximation to an FEA determined value of k_{i2} can be obtained from the assumption that the low frequency capacitance follows eq. (4). Determining the capacitance with and without the piezoelectric effect active should thus be sufficient. The analytic value equals that in Appendix 1.

As can seen, extracting the information from the FEA simulations is just like extracting information from any experimentally derived curves.

Three different sets of piezoelectric constants were used for the simulations. The full set of material constants has been complemented by two reduced sets. The simulation in which all piezoelectric constants are set equal to zero is used to obtain a reference value of the resonance frequency. The simulation in which only d_{32} (PZT) and d_{12} (quartz) are non-zero represents the analytic case. The d_{ik} components were set equal to zero before the e_{ik}-matrix was determined. That the results change slightly when the "unimportant" piezoelectric components are activated is due to them "stealing" some energy.

Most of the deviation between the FEA and the analytic results in Tables 3 to 7 can be compensated for by adjusting the values of $\dot{\vartheta}_d$ and $\dot{\vartheta}_p$. This corresponds to the location of the electrodes differing slightly between the models. For the analytic approach, it was assumed that there was no gap between near-lying electrodes. The finite element model has, per definition, an element size dependent gap. The gap-size is most important for the electrode configuration in Figure 6c since its gap is located where the density of bound piezoelectric charges is largest.

A finer mesh than the 10×6×6 mesh used in the simulations would reduce the difference due to the unintentional electrode gap. It would also reduce the difference between the FEA determined and the actual electric field. Altering the gap-size and the element size in the two-dimensional FEA-calculation of $\dot{\vartheta}_d$ and $\dot{\vartheta}_p$ verifies that this is the main reasons for the deviation between the FEA and analytic results.

However, using a finer mesh results in longer CPU-times, especially since the piezoelectric elements are CPU-intensive. To illustrate the CPU-times involved for piezoelectric simulations, the electric DOFs were disabled for SOLID5 during a modal analysis. This reduced the CPU-time from 165 to 50 seconds, including model generation and plotting of the results. Correspondingly, deactivating the mechanical DOFs when calculating the dielectric capacitance reduced the CPU-time from 120 to 20 seconds. The simulations were made using ANSYS 5.1 on a 90 MHz PC-Pentium with 32 MB internal memory.

The length of the beam is ten times the dimensions of the cross-section. This means that classical beam theory can be

expected to predict the behavior accurately if the beam is free to move in the cross-section. For the FEA model, this assumption is not valid near the mounting of the beam since the beam there is clamped in all three directions. A slightly lower deflection derived with the FEA model can thus be expected. However, this does not explain the deviation between the FEA and the analytic results since the deviation varies between different electrode configurations and vibration directions.

Figure 9 illustrates the voltage field within the material at resonance. The large voltage in the figure to the right are generated by the mechanical deformation of the material. This is the concluding example that three-dimensional FEA can be used to study effects that are not easily treated with other methods, to visualize these effects, and to determine their effect on other parameters.

6. DISCUSSION

In conclusion, the comparison of the results from the FEA and the analytic approaches shows that FEA describes the piezoelectric well. The results have also been compared successfully with experiments (Söderkvist 1991b, Söderkvist and Hjort 1993). For instance, measured values of R_1 for quartz tuning forks were between 0 and 7% higher than those predicted, which was in the same order as the accuracy of the measurements. This implies a maximum error in the value of $\hat{u}_1$ of 3.4%.

The FEA and analytic-FEA approaches complement each other well. Carrying out all simulations with piezoelectric elements is normally too time-consuming. Using the analytic-FEA approach during part of the design phase is a more time and computer efficient solution.

In this study, only bending modes are studied. However, similar tests have been carried out successfully also for shear vibrations.

The results are important for, for instance, the design of structures produced by micromachining techniques. There, the geometries are fairly simple, but the device possibilities are numerous despite this. To use the possibilities to their fullest extent, a detailed understanding of the underlying principles is essential. This is more important for smaller structures since finding the actual behavior from measurements can be a very difficult, costly and time-consuming.

A well-known example of a successful micromachined piezoelectric device is the small quartz tuning fork used for time-keeping in watches. For such a device, the simulations can be used, for instance, for finding the orientation of the tuning fork relative the crystallographic coordinate system that gives optimum temperature behavior. Such simulations need relative accuracy of the FEA determined resonance frequencies of better than 1 ppm, and will include up to third order temperature coefficients of the anisotropic material parameters. Suppressing the excitation of overtones and the optimization of C_1/C_o as a function of electrode location in the direction of the tines are two additional examples for which the (analytic-)FEA approach is well suited (Söderkvist 1991c).

APPENDIX 1

The following material parameters were used in the calculations (Vernitron 1983, James 1988):

	PZT 4	*Quartz*
$s_{11}= s_{22}$ [m^2/N]	$12.3\cdot10^{-12}$	$12.78\cdot10^{-12}$
$e_{11}/e_o= e_{22}/e_o$	1475	4.51
e_{33}/e_o	1300	4.63
$d_{11} = -d_{12}$ [C/N]	-	$2.3\cdot10^{-12}$
$d_{31} = d_{32}$ [C/N]	$-123\cdot10^{-12}$	-
$k_{11} = k_{12}$ [%]	-	10.2
$k_{31} = k_{32}$ [%]	-33	-
r [kg/m^3]	7500	2648
Q_1	500	10,000

TABLE 8. Material parameters used in the simulations.

It is assumed that the piezoceramic material is poled along the z-direction.

The order in which the material parameters are given in literature and in ANSYS differ. For instance, the piezoelectric constant matrix, d_{ik}, for quartz is given in the literature as:

$$d_{ik}(\text{literature}) = \begin{pmatrix} d_{11} & -d_{11} & 0 & d_{14} & 0 & 0 \\ 0 & 0 & 0 & 0 & -d_{14} & -2d_{11} \\ 0 & 0 & 0 & 0 & 0 & 0 \end{pmatrix} \quad \text{(A1)}$$

while the parameters should be input in ANSYS with columns 4, 5 and 6 permutated, i.e., with the following order:

$$d_{ik}(\text{ANSYS}) = \begin{pmatrix} d_{11} & -d_{11} & 0 & 0 & d_{14} & 0 \\ 0 & 0 & 0 & -2d_{11} & 0 & -d_{14} \\ 0 & 0 & 0 & 0 & 0 & 0 \end{pmatrix} \quad \text{(A2)}$$

Rows and columns 4, 5 and 6 of the stiffness matrix should be permutated correspondingly.

REFERENCES

Benjaminson, A. and Stallings, S.C., 1989, "A Microcomputer-Compensated Crystal Oscillator using a Dual-Mode Resonator," Proc. 43th Ann. Symp. on Frequency Control, IEEE: 89CH2690-6, pp. 20-26.

Benes, E., Gröschl, M., Burger, W. and Schmid, M., 1995, "Sensors Based on Piezoelectric Resonators," Sensors and Actuators A, Vol. 48, pp. 1-21.

Chen, Q.X. and Payne, P.A., 1995, "Industrial Applications of Piezoelectric Polymer Transducers," Meas. Sci. Technol., Vol. 6, pp. 249-267.

Danel, J.S. and Delapierre, G., 1991, "Quartz: A Material For Microdevices," J. Micromech. Microeng., Vol. 1, pp. 187-198.

EerNisse, E.P., Ward, R.W. and Wiggins, R.B., 1988, "Survey of Quartz Bulk Resonator Sensor Technologies," IEEE Trans. Ultrasonics, Ferroelectrics, and Frequency Control, Vol. 35, pp. 323-330.

Gallego-Juárez, J.A., 1989, "Piezoelectric Ceramics and Ultrasonic Transducers," J. Phys. E: Sci. Instrum., Vol. 22, pp. 804-816.

James, B.J., 1988, "A New Measurement of the Basic Elastic and Dielectric Constants of Quartz," Proc. 42nd Annual Symp. on Frequency Control, IEEE: 88CH2588-2, pp. 146-154.

Kunisch, C. and Holleck, H., 1995, "Design of Piezoelectric Thin Films in the System AIN-ZnO," To be published in Surf. Coat. Techn.

Marcus, M.A., 1981, "Ferroelectric Polymers and their Applications," Proc. 5th Int. Meeting on Ferroelectricity at Pennsylvania State Univ.

Meldrum, M.A., 1990, "Application of Vibrating Beam Technology to Digital Acceleration Measurement," Sensors and Actuators A, Vol. 21-23, pp. 377-380.

Pointon, A.J., 1982, "Piezoelectric Devices," *IEE Proc.*, Vol. 129 Pt. A, pp. 285-307.

Smith, W.A., 1992, "New Opportunities in Ultrasonic Transducers Emerging from Innovations in Piezoelectric Materials," Proc. SPIE, Vol. 1733, pp. 3-26.

Studer, B. and Zingg, W., 1990, "Technology and Characteristics of Chemically Milled Miniature Quartz Crystals," Proc. 4th European Frequency and Time Forum, Neuchâtel, Switzerland.

Söderkvist, J., 1990, "Electric Equivalent Circuit for Flexural Vibrations in Piezoelectric Materials," IEEE Trans. Ultrasonics, Ferroelectrics, and Frequency Control, Vol. 37, pp. 577-586.

Söderkvist, J., 1991a, "Dynamic Behavior of a Piezoelectric Beam," J. Acoust. Soc. Am., Vol. 90, pp. 686-692.

Söderkvist, J., 1991b, "A Phenomenological Method of Predicting the Performance of Piezoelectric Beams," J. Micromech. Microeng., Vol. 1, pp. 16-24.

Söderkvist, J., 1991c, "Piezoelectric Beams and Vibrating Angular Rate Sensors," IEEE Trans. Ultrasonics, Ferroelectrics, and Frequency Control, Vol. 38, pp. 271-280.

Söderkvist, J. and Hjort, K., 1993, "Flexural Vibrations in Piezoelectric Semi-Insulating GaAs," Sensors and Actuators A, Vol. 39, pp. 133-139.

Söderkvist, J., 1994, "Micromachined Gyroscopes," Sensors and Actuators A, Vol. 43, pp. 65-71.

Söderkvist, J., 1995, "Limitations to the Piezoelectric Effect for Materials with Finite Resistivity," Proc. Transducers '95, Vol. 2, ISBN 91-630-3473-5, paper 285.

Vernitron Piezoelelctric Division, 1983, "Piezoelelctric Technology Data for Designers," Bedford, Ohio, U.S.A.

Young, W.C., 1989, "Roark's Formulas for Stress & Strain," 6th ed., McGraw-Hill, New York, p. 714.